Quantum dynamics with short-time trajectories and minimal adaptive basis sets

Maximilian A. C. Saller and Scott Habershon*

Department of Chemistry and Centre for Scientific Computing, University of Warwick, Coventry, CV4 7AL, United Kingdom

E-mail: S.Habershon@warwick.ac.uk

Abstract

Methods for solving the time-dependent Schrödinger equation *via* basis set expansion of the wavefunction can generally be categorised as having either static (time-independent) or dynamic (time-dependent) basis functions. We have recently introduced an alternative simulation approach which represents a middle road between these two extremes, employing dynamic (classical-like) trajectories to create a static basis set of Gaussian wavepackets in regions of phase-space relevant to future propagation of the wavefunction [*J. Chem. Theory Comput.*, **11**, 8 (2015)]. Here, we propose and test a modification of our methodology which aims to reduce the size of basis sets generated in our original scheme. In particular, we employ short-time classical trajectories to continuously generate new basis functions for short-time quantum propagation of the wavefunction; to avoid the continued growth of the basis set describing the time-dependent wavefunction, we employ Matching Pursuit to periodically minimize the number of basis functions required to accurately describe the wavefunction. Overall, this approach generates a basis set which is adapted to evolution of the wavefunction whilst also being as small as possible. In applications to challenging benchmark problems, namely a 4-dimensional model of photoexcited pyrazine and three different double-well tunnelling problems, we find that our new scheme enables accurate wavefunction propagation with basis sets which are around an order-of-magnitude smaller than our original trajectory-guided basis set methodology, highlighting the benefits of adaptive strategies for wavefunction propagation.

1 Introduction

The key challenge of wavefunction-based quantum dynamics lies in solving the time-dependent Schrödinger equation (TDSE),[1]

$$-i\hbar \frac{\partial}{\partial t} |\psi(\mathbf{q},t)\rangle = \hat{H} |\psi(\mathbf{q},t)\rangle \ , \tag{1}$$

where $\mathbf{q}$ describes the nuclear degrees-of-freedom and $\hat{H}$ is the Hamiltonian operator (defined as the sum of kinetic and potential contributions, $\hat{H} = \hat{T} + \hat{V}$). Most commonly, the time-dependent wavefunction $|\psi(\mathbf{q},t)\rangle$ is approximated as a linear expansion in a set of basis function, $|\phi(\mathbf{q},t)\rangle$,

$$|\psi(\mathbf{q},t)\rangle = \sum_{i=1}^{N} c_i(t) |\phi_i(\mathbf{q},t)\rangle \ . \tag{2}$$

Quantum dynamics methods relying on this approach can be categorised based on the manner in which the basis set behaves. Basis functions may be chosen at the outset, resulting in a time-independent basis set, $|\phi_i(\mathbf{q},t)\rangle = |\phi_i(\mathbf{q})\rangle$. Once sampled, the basis functions remain static, and the time-dependence of the system is expressed through propagation of the expansion coefficients, $c_i(t)$,[2–4] according to the Dirac-Frenkel variational principle.[5–8] Because the basis functions are time-independent, the region of phase-space spanned by the basis set must be carefully chosen at the start of a calculation; the most direct implementation of this approach, whereby the entire phase-space of interest is spanned by the basis set, leads to the well-known exponential scaling with system size.[9]

Alternatively, time-dependent basis sets feature basis functions, $|\phi_i(\mathbf{q},t)\rangle$, which adapt to follow wavefunction evolution in time;[10,10–12,12–25] in general, the associated expansion coefficients, $c_i(t)$, are again propagated using the Dirac-Frenkel variational principle.[5–8] To date, a wide range of time-dependent basis functions, as well as a variety of different equations-of-motion for the basis functions themselves, have been employed in quantum dynamics simulations. With regards to basis sets evolving under variational equations-of-motion, the

most prominent example is the multi-configurational time-dependent Hartree (MCTDH) approach, which employs expansion of the wavefunction in terms of single-particle functions, yielding highly accurate results at reasonable computational expense.[10,10–13] In the related G-MCTDH method, single-particle functions in selected (environmental) degrees-of-freedom are replaced with Gaussian wavepackets (GWPs);[14] this development is taken to its natural conclusion in the variational multiconfigurational Gaussian (vMCG) method, where the basis functions are multidimensional GWPs which evolve according to variational equations-of-motion.[12,15–19] While these variational methods for propagating basis functions are increasingly applied to high-dimensional problems, challenges remain; for example, MCTDH requires that the potential energy surface (PES) of interest be expressed as a sum of product terms, requiring a prior non-trivial fitting procedure, while the equations-of-motion of vMCG can be ill-conditioned, such that convergence with respect to basis set size can itself become challenging.

The challenges of variational evolution can be alleviated somewhat by employing non-variational equations-of-motion which are easier to deal with from a computational viewpoint. For example, the *ab initio* multiple spawning (AIMS) method[23,25,26] evolves a time-dependent set of GWP basis functions using classical molecular dynamics, while a novel algorithm is employed to adaptively expand the basis set as non-adiabatic events are detected. Combined with on-the-fly evaluation of adiabatic electronic states and couplings, the AIMS methodology has enabled direct insight into the photorelaxation in complex environments.[25,27] The multi-configurational Ehrenfest (MCE) method[28,29] developed by Shalashilin and coworkers employs a similar approach, but here the basis functions simultaneously span multiple electronic states and evolve according to Ehrenfest trajectories; most recently, the ideas of AIMS and MCE have been combined in the *ab initio* multiple cloning algorithm,[30] which has already been employed to investigate photodissociation phenomena in organic chromophores. We also note that the recently published quantum trajectory Gaussian basis (QTGB)[9] method provides an interesting perspective in its application of Bohmian mechan-

ics to its guiding trajectories; initial applications of this approach to two-dimensional problems have proven promising, while the applicability to more challenging higher-dimensional systems remains to be tested. Expanding the scope further beyond trajectory-guided methods for wavefunction propagation, there also exist a range of methods which employ mixed strategies whereby a quantum sub-system evolves in the presence of a classical environment; the quantum wavepacket *ab initio* molecular dynamics (QWAIMD) method[31,32] is a good example of such an approach which has found application to, for example, vibrational properties of hydrogen-bonded dihalide systems.[33] Of course, the idea of classical evolution of wavefunctions is also tied to the enormous range of work on semi-classical quantum dynamics methods, including the popular linearized- semi-classical initial value representation (LSC-IVR[34–39]) and forwards-backwards IVR methods (FB-IVR[40,41]) which have been successfully employed to study systems ranging from liquid water[42] to photosynthetic complexes.[39]

While these, and other, non-variational approaches to wavefunction propagation have been shown capable of providing new insights into quantum dynamics of complex systems, they are not without problems; for example, approximate (non-variational) equations-of-motion can violate the energy-conservation implicit in the TDSE.[43] Furthermore, the propagation of basis functions based on *classical* equations-of-motion is potentially inadequate in capturing all dynamical effects; in the most challenging cases, these simulations can fail to sample the regions of configurational space associated with tunnelling, unless some care is given to the choice of initial conditions for the basis function trajectories.

As a result of the remaining computational challenges associated with both variational and non-variational quantum simulation approaches, there remain opportunities for developing new strategies. One strategy which our group, and others,[4,9,44,45] have begun to explore is the idea of *adaptive* basis sets which represent a "middle road" between time-dependent and time-independent basis set strategies. Here, the individual basis functions describing the wavefunction are time-independent, but the basis functions themselves are adaptively added or removed from the full basis set as the wavefunction evolves; the time-evolution

of the expansion coefficients associated with the static basis functions is performed variationally, thereby circumventing the problem of energy conservation encountered by non-variational evolution. Within this class of methods, the matching pursuit split operator Fourier transform (MP-SOFT)[46,47] approach is perhaps most successful to date. Here, a "greedy" matching pursuit (MP) algorithm is employed to transform between grid-based and GWP-based representations of a time-dependent wavefunction, enabling efficient analytical evolution under the operation of the kinetic energy operator. However, the potential energy operator in MP-SOFT must still be expressed on a uniform grid in configurational space; this approach is therefore at odds with the demands of "direct" quantum dynamics approaches which are interfaced with *ab initio* electronic structure methods. More recently, the basis expansion leaping (BEL)[45] method avoids the use of a grid in configurational space completely, and instead exploits the over-complete nature of GWP basis sets. Here, a basis set of GWPs is periodically expanded by placing new GWP basis functions into empty regions of phase-space according to an overlap-based metric; following variational evolution of the expansion coefficients, the GWP basis set is periodically pruned to remove redundant GWPs. This approach has demonstrated good initial performance for a two-dimensional benchmark problem, but has not yet been employed to higher-dimensional systems. Further examples of basis adaptation strategies have employed ideas based on identifying linear dependence through analysis of overlap matrices and subsequently employing methods such as singular value decomposition (SVD); recent work by Prociuk and, separately, Worth are good examples within this category.[48,49]

In the spirit of these adaptive approaches, we have recently introduced a novel method for basis set generation for quantum dynamics.[44] Here, we employ computationally-simple (classical molecular dynamics or Ehrenfest-type) trajectories to place GWP basis functions in phase-space, guided by the PES of the system. Following the initial sampling stage, the GWP basis set behaves time-independently, with wavefunction propagation being expressed variationally through the expansion coefficients. In contrast to the BEL method, our strat-

egy employs a physically-motivated placement of basis functions, albeit at the additional cost of running multiple sampling trajectories. Our trajectory-guided method was very successfully applied to the vibronic Hamiltonian models describing the decay of photoexcited pyrazine, resulting in qualitative reproduction of exact MCTDH dynamics for both 4- and 24-dimensional representations.

Given the simplicity of this strategy for sampling GWP basis functions for quantum dynamics basis sets, these initial results were encouraging; however, we recognise a number of important assumptions associated with our initial methodology. Chief among these assumptions is that the *classical* trajectories employed during the basis sampling stage will explore the same regions of phase-space which are relevant to *quantum* propagation; however, classical trajectories can potentially sample regions of phase-space which are inconsistent with quantum mechanics, for example due to their inability to correctly treat zero-point energy (ZPE)[50–52] and tunnelling, as already noted above.

To overcome these challenges, this Article proposes a modification to our initial trajectory-guided method. In particular, we adopt the view that classical trajectories with appropriate initial conditions are suited to sample basis functions for short time-periods; this is in contrast to our initial report, where classical molecular dynamics trajectories are assumed to sample the relevant region of phase-space for quantum propagation over the entire simulation time-scale. Thus, we retain both the strategy for sampling basis functions as well as the time-independent propagation algorithm, however we now split the full time-evolution into small segments, each requiring short "bursts" of GWP basis function sampling, followed by propagation of the expansion coefficients according to the TDSE. Between these trajectory bursts, we employ the MP algorithm[23,27,30,53–55] to minimise the active basis set and optimise the wavefunction representation quality. Overall, our scheme evolves a quantum wavefunction using repeated expansion (*via* classical trajectories) and minimization (*via* MP); the main conclusion of this paper is that this adaptive scheme allows for the simulation of qualitatively accurate quantum dynamics in many-dimensional systems at a fraction of

the computational expense of our initial basis-set sampling strategy.

2 Theory

2.1 Original trajectory-guided sampling scheme

To set the context for the adaptive basis strategy introduced here, we first outline our original trajectory-guided approach.[44] We assume that our system of interest is described by f nuclear degrees-of-freedom and a set of diabatic states $|\alpha\rangle$, and we assume that we have an initial wavefunction $|\psi(\mathbf{q},0)\rangle|\alpha\rangle$. We subsequently initialise a set of m trajectories with initial conditions chosen based on the characteristics of the initial wavefunction; for example, the initial positions and momenta of each trajectory could be drawn from the Wigner distribution of the initial wavefunction. These trajectories are then propagated for n_t time-steps according to either classical or Ehrenfest trajectories, depending upon the number of electronic states in the system. Along each trajectory, the coordinates and momenta of the current phase-space point are stored at each time-step with a probability of $1/n_s$, where n_s is a user-defined frequency factor which, along with m, influences the total basis set size; in the case of systems containing multiple electronic states, we note that we place a GWP basis function on each electronic state such that the total basis set scales linearly with number of electronic states.

The TDSE is subsequently solved using the entire set of $N \simeq m \times (n_t/n_s)$ basis functions which, for the sake of computational simplicity, are chosen to be f-dimensional GWPs of the form,

$$\langle \mathbf{q}|g_j\rangle = N_j e^{-(\mathbf{q}-\mathbf{q}_j)^{\mathrm{T}}\mathbf{A}_j(\mathbf{q}-\mathbf{q}_j)+\frac{i}{\hbar}\mathbf{p}_j\cdot(\mathbf{q}-\mathbf{q}_j)}, \tag{3}$$

where N_j is the GWP normalisation constant, $\mathbf{A}_j$ is an $f \times f$ diagonal matrix with entries $\gamma_\kappa/\hbar$, where κ labels the degree-of-freedom, and $\{\mathbf{q}_j, \mathbf{p}_j\}$ are the position and momenta of the corresponding trajectory. Again, for computational simplicity, we use fixed-width GWPs,

such that γ_κ is a constant for each degree-of-freedom κ.

Using the full basis set of N GWPs, the wavefunction of the system is subsequently written as

$$|\psi(\mathbf{q};t)\rangle = \sum_{j=1}^{N} c_j(t)|g_j\rangle|\alpha_j\rangle, \tag{4}$$

where we note that the sampled GWPs are now assumed to be time-independent, with the time-dependence of $\psi(\mathbf{q};t)$ carried solely through the expansion coefficients. Direct application of the Dirac-Frenkel variational principle yields

$$\dot{\mathbf{c}} = -\frac{i}{\hbar}\mathbf{S}^{-1}\mathbf{H}\mathbf{c}, \tag{5}$$

where $\mathbf{S}$ is the overlap matrix with elements

$$S_{ij} = \langle\alpha_i|\langle g_i|g_j\rangle|\alpha_j\rangle, \tag{6}$$

and $\mathbf{H}$ is the Hamiltonian matrix with elements

$$H_{ij} = \langle\alpha_i|\langle g_i|\hat{H}|g_j\rangle|\alpha_j\rangle, \tag{7}$$

for the set of N basis functions.

2.2 Adaptive trajectory-guided scheme

While the trajectory-guided strategy outlined above was proven to be successful in simulations of 4- and 24-dimensional models of photorelaxation in pyrazine, as well as in 50-dimensional simulations of a spin Boson model,[44] there are two drawbacks to the strategy. First, using classical-like trajectories to sample GWP basis functions can lead to inconsistencies in the regions of phase-space sampled by the basis set and those most relevant to quantum propagation; most importantly, as already noted above, this might arise when one

considers tunnelling problems, where classical trajectories might not be able to cross barriers on the PES which might otherwise be traversed in full quantum simulations. Furthermore, classical trajectories with initial conditions sampled from a quantum phase-space distribution can lead to ZPE leakage,[56] where the ZPE in bound vibrational modes escapes into the remaining degrees-of-freedom of the system, violating the conservation of ZPE implicit in quantum dynamics. We emphasize here that this potential ZPE leakage problem is not associated with the wavefunction propagation itself, which is performed by variational evolution of the TDSE within our approaches, but is associated with the use of a finite set of classical trajectories which are not guaranteed to sample the correct quantum phase-space distribution once propagated in time. A second drawback of our original strategy is that the total size of the basis set generated by our trajectory-sampling approach can be quite large. For example, in applications to the 4-dimensional model of photoexcited pyrazine, it was found that around 24×10^3 basis functions were required to give quantitative agreement with accurate MCTDH results for the time-dependent populations of the diabatic states.

These challenges can, in principle, be addressed introducing two modifications into our original sampling strategy. First, we replace the long-time classical trajectory sampling of our original method with multiple short-time trajectories. By using classical-like trajectories to sample GWP basis functions relevant to short-time (*i.e.* tens of femtoseconds) quantum propagation, we minimize the ZPE leakage problem, which is typically observed in simulations on longer timescales (*i.e.* few 100 femtoseconds to picoseconds, depending on the system). Furthermore, by repeatedly restarting new trajectories with initial conditions drawn from the current wavefunction $\psi(\mathbf{q};t)$, we improve the likelihood of sampling basis functions which are relevant to quantum dynamics in the immediate future, without having to sample potentially superfluous basis functions at longer times. The second improvement to our initial strategy is to introduce a scheme to adaptively prune the basis set during the calculation; this is necessary to avoid the continuous expansion of the basis set which would arise by continued propagation of trajectories. In this work, we exploit the

over-complete nature of GWP basis sets,[43] to adaptively create a minimal basis set which accurately represents the time-dependent wavefunction with as few GWP basis functions as possible. As already noted, this adaptive strategy has been employed in several previous GWP-based simulations;[9,43,45] however, our approach is unique in using MP to generate a minimal representation of the wavefunction while avoiding linearly-dependent GWP basis functions.

Introducing the two changes outlined above into our original strategy gives a new approach founded on short-time trajectories and automated basis adaptation. In the remainder of this paper, we focus on comparing our original strategy, referred to hereafter as standard trajectory-guided (sTG), to the modified strategy, referred to hereafter as adaptive trajectory-guided (aTG). In summary, as shown in Fig. 1, our aTG scheme for wavefunction propagation proceeds as follows:

1. Assume that we have a wavefunction at some time t, $|\psi(\mathbf{q};t)\rangle$, given as a linear combination of N GWPs, as in Eq. 4.

2. Sample m sets of appropriate initial positions and momenta from the current wavefunction. To sample each of the m initial conditions, we select a GWP k with a probability given by the magnitude of its overlap onto the total wavefunction, $|\langle g_k|\psi(\mathbf{q};t)\rangle|$; for the selected GWP, initial position and momenta are sampled from the Wigner distribution of the $|g_k\rangle$.

3. Using the sampled initial conditions, propagate m trajectories for a short time t_s using classical molecular dynamics (in the case of a single diabetic surface), Ehrenfest dynamics (multistage case), or any other appropriate classical-like approach.

4. Along each sampling trajectory, place fixed-width GWPs at the current phase-space point $(\mathbf{q}_j, \mathbf{p}_j)$ with a probability $1/n_s$ at each propagation time-step.

5. The sampled GWPs are added to the set of N original GWPs, with the expansion

coefficients of the new GWPs set to zero; the total size of the new GWP basis set is N^I.

6. The expansion coefficients of the N^I GWPs are now propagated according to Eq. 5 for time t_s.

7. Following propagation, use MP to minimize the size of the GWP basis set, while still accurately representing the current wavefunction. This results in a new set of N^B GWPs describing the wavefunction, and we then go back to step (1).

As is clear from Fig. 1, this strategy results in a wavefunction which constantly expands and contracts throughout the quantum propagation; in contrast to our original sTG approach, the results below show that this adaptive strategy dramatically reduces the total size of the basis set required in a given quantum dynamics problem, without compromising simulation accuracy. However, to complete the description of our aTG approach, we now outline the MP strategy as implemented here to periodically generate a minimal GWP representation of a time-dependent wavefunction.

2.3 The matching pursuit optimisation algorithm

Our aTG strategy uses MP to periodically minimize the size of the GWP basis required to describe the current wavefunction. The MP strategy as implemented here exploits the fact that the GWP basis set is overcomplete; MP then allows us to find a wavefunction representation which requires as few GWP basis functions as possible. In this way, periodic application of MP allows us to adaptively minimize the overall basis set size, leading to fewer evaluations of overlap and Hamiltonian matrix elements and a more efficient simulation overall. In this work, we use the MP algorithm[53] to minimise and optimise the active basis set at the end of each trajectory-sampling period, following propagation of the basis expansion coefficients; the resulting minimal basis set is then used as the initial wavefunction for the next short-time period of basis set sampling and propagation.

Originally a method for signal decomposition,[53] MP has also found previous applications in quantum dynamics simulations,[43,46,47,57] most notably in the MP-SOFT method. MP is a "greedy" algorithm for selecting, from a large set of basis functions, the minimal set of functions required to reproduce a target signal (or, in the present context, wavefunction) with a chosen accuracy. The MP procedure implemented here can be summarised as follows:

1. Let
$$\left|\psi^A(\mathbf{q},t)\right\rangle = \sum_i^{N^I} c_i^A(t)\left|\phi_i^A(\mathbf{q})\right\rangle$$
be the wavefunction at time t. Note that the wavefunction is described by N^I GWP basis functions and their associated diabatic state, $|\phi_i(\mathbf{q})\rangle = |g_i(\mathbf{q})\rangle|\alpha_i\rangle$; these N^I GWPs form the set $\{\phi^A\}$.

2. Store the initial wavefunction: $\left|\psi^I(\mathbf{q},t)\right\rangle = \left|\psi^A(\mathbf{q},t)\right\rangle$.

3. Initialise the number of GWPs in the minimal description of the current wavefunction: $N^B = 0$. Also, initialize the set $\{\phi^B\}$, containing GWPs which comprise the MP-optimized description of the wavefunction $\left|\psi^A(\mathbf{q},t)\right\rangle$; initially, the set $\{\phi^B\}$ is empty.

4. Select from the current set of GWPs, $\{\phi^A\}$, the GWP possessing the largest absolute overlap
$$\omega = |\left\langle\phi^A(\mathbf{q})\right|\left.\psi^A(\mathbf{q},t)\right\rangle|$$
with the active wavefunction $\left|\psi^A(\mathbf{q},t)\right\rangle$.

5. Maximise the overlap function ω with respect to the parameters of GWP $\left|\phi^A(\mathbf{q})\right\rangle$ (namely, positions $\mathbf{q}_A$ and momenta $\mathbf{p}_A$), using a suitable algorithm such as steepest-descents or conjugate gradients.

6. The optimised GWP basis function, ϕ_{opt}, is added to the set of retained basis functions which will be used to form the minimal description of the wavefunction $\left|\psi^A(\mathbf{q},t^A)\right\rangle$. Increment the new GWP set: $N^B \to N^B + 1$, $\{\phi^B\} \to \{\phi^B\} + \phi_{\text{opt}}$.

7. Calculate new expansion coefficients, $c^B(t)$, for the minimal representation defined by the set $\{\phi^B\}$,

$$\left|\psi^B(\mathbf{q},t^B)\right\rangle = \sum_i^{N^B} c_i^B(t)\left|\phi_i^B(\mathbf{q})\right\rangle \,.$$

The expansion coefficients can be determined by projection of the N^B GWP basis functions onto $\left|\psi^A(\mathbf{q},t)\right\rangle$. Thus,

$$\mathbf{c}^B(t) = \left(\mathbf{S}^B\right)^{-1}\mathbf{W}\,,$$

where $\mathbf{S}^B$ is the $N^B \times N^B$ overlap matrix for the optimised set of GWPs and $\mathbf{W}$ is a vector of length N^B with elements $W_j = \langle\phi^B|\psi^A\rangle$.

8. Update the remainder of the wavefunction by subtracting the optimized counterpart, such that

$$\left|\psi^A(\mathbf{q},t^A)\right\rangle \rightarrow \sum_i^{N^I} c_i^A(t)\left|\phi_i^A(\mathbf{q})\right\rangle - \sum_i^{N^B} c_i^B(t)\left|\phi_i^B(\mathbf{q})\right\rangle$$

.

9. Check convergence of the minimal representation. If the norm of the overlap of the optimised representation onto the initial wavefunction is greater than a user-defined cut-off Δ, such that

$$|\left\langle\psi^B(\mathbf{q},t)\right|\left.\psi^I(\mathbf{q},t)\right\rangle| \geq \Delta\,,$$

then replace the wavefunction $\left|\psi^I(\mathbf{q},t)\right\rangle = \left|\psi^B(\mathbf{q},t)\right\rangle$ and continue propagation. Otherwise, go to step (4).

The wavefunction resulting from this MP procedure typically contains far fewer GWPs than the initial wavefunction, yet reproduces the original wavefunction to an accuracy described by Δ. An example of this is shown in Fig. 2, wherein the sizes N^I and N^B are compared for a simulation of the 4-dimensional pyrazine model (details given below).

As a final point, it is worth commenting on the additional computational expense incurred

by this adaptive MP scheme. Depending on the frequency with which MP is performed on the current active basis set, as well as the size of the basis set itself, we find that MP represents a significant increase in the overall computation time when one is using simple analytical PESs. However, it is important to bear in mind that our long-term goal is to use our GWP propagation scheme in "on-the-fly" quantum dynamics, where the PES is evaluated using *ab initio* electronic structure calculations during the course of the time-evolution, rather than pre-fitting an analytical PES to a database of prior electronic structure calculations. In this "on-the-fly" scenario, the additional expense of MP is expected to be small compared to the benefits which will arise from propagating the wavefunction using a minimal basis set; in particular, by minimizing the size of the basis set, we ultimately minimize the number of (computationally demanding) *ab initio* electronic structure calculations which will be required for evaluation of the Hamiltonian matrix.

3 Results and discussion

The aTG scheme outlined above improves upon our original sTG scheme by reducing the dependence on the accuracy of classical dynamics and introducing an adaptive scheme for selecting a minimal basis set. In this Article, we focus on assessing the impact of these two changes by considering quantum dynamics simulations of three different systems: (i) non-adiabatic dynamics in a 4-dimensional model of pyrazine following photoexcitation to the S_2 electronic state, (ii) tunnelling in a double-well potential with linearly-coupled degrees-of-freedom, and (iii) tunnelling in a double-well potential with strong non-linear coupling to the tunnelling coordinate. These systems are selected because they each represent challenging prototypical problems in quantum dynamics, yet analytical PESs and numerically exact benchmark results are available; furthermore, we emphasize that our ultimate goal is to model quantum dynamics in complex multidimensional systems, so we prefer to benchmark new methodologies for challenging problems in preference to 1- or 2-dimensional cases.

3.1 Photorelaxation in pyrazine

Pyrazine, $C_4H_4N_2$, exhibits vibronic coupling between its first and second excited electronic states, S_1 and S_2 respectively. As a result of this, photoexcitation to S_2 from the ground state, S_0, is followed by ultrafast population transfer to S_1. The ultrafast relaxation between these states is ascribed to the presence of a conical intersection between S_2 and S_1, resulting in a broad photoabsorption spectrum with few sharply-defined features.[58–60]

This pyrazine system has evolved into a benchmark problem for non-adiabatic dynamics. In particular, a vibronic Hamiltonian is available which has been fit to experimental data and *ab initio* calculations, and this Hamiltonian has been used in extensive MCTDH simulations, thereby providing benchmark results for comparison. The 24-dimensional, two electronic-state vibronic Hamiltonian can be written as[13]

$$\begin{aligned}\hat{\mathrm{H}} = &\sum_{i=1}^{f}\left[-\frac{\omega_i}{2}\frac{\partial^2}{\partial q_i^2}+\frac{\omega_i}{2}q_i^2\right]+\begin{pmatrix}-\Delta & 0\\ 0 & \Delta\end{pmatrix}+\sum_{i\in G_1}\begin{pmatrix}a_i & 0\\ 0 & b_i\end{pmatrix}q_i \\ &+\sum_{(i,j)\in G_2}\begin{pmatrix}a_{ij} & 0\\ 0 & b_{ij}\end{pmatrix}q_iq_j+\sum_{i\in G_3}\begin{pmatrix}0 & c_i\\ c_i & 0\end{pmatrix}q_i+\sum_{(i,j)\in G_4}\begin{pmatrix}0 & c_{ij}\\ c_{ij} & 0\end{pmatrix}q_iq_j\,,\end{aligned} \tag{8}$$

where q_i is the normal-mode coordinate of the ith vibrational mode and ω_i represents the corresponding vibrational frequency. The energy splitting between S_1 and S_2 is equal to 2Δ at the origin of nuclear coordinate-space. The known parameters a_i, b_i, a_{ij} and b_{ij} describe linear and bilinear expansion terms, while the coupling between states is expressed by c_i and c_{ij}. The subdivision of vibrational modes in Eq. 8 reflects the symmetry of the system; the mode coupling the S_1 (B_{2u}) and S_2 (B_{3u}) states must possess B_{1g} symmetry. The set G_1 thus contains all modes of A_g symmetry, G_2 is comprised of pairs of modes with identical symmetry, G_3 represents a single mode with B_{1g} symmetry and G_4 is the set of all pairs of modes, the product of which results in B_{1g} symmetry.

The four-dimensional ($f = 4$) version of this Hamiltonian, comprising the vibronic cou-

pling mode ν_{10a} and the three A_g modes exhibiting the strongest linear coupling (ν_1, ν_{6a} and ν_{9a}), is well-known to sufficiently represent the population dynamics of the photoexcited system.[44] This significantly reduces the computational challenge in comparison with explicit treatment of all 24 vibrational modes. As our previous work[44] was mostly focussed on this lower-dimensional model, we will limit ourselves to discussion of the 4-mode Hamiltonian here. It is worth noting that even this lower dimensional version of the full Hamiltonian exceeds the the size of systems for which other adaptive basis methods such as BEL[45] and QTGB[9] have been demonstrated to date.

To sample basis functions, we retain the propagation scheme used in our previous work,[44] relying on mean-field Ehrenfest equations-of-motion which account for multiple electronic states. Thus each sampling trajectory represents a basis function of the form,

$$|\phi(\mathbf{q},t)\rangle = \left[a_1(t)\,|1\rangle + a_2\,|2\rangle\right]|g_t(\mathbf{q}_t,\mathbf{p}_t)\rangle\ , \tag{9}$$

where $a_{1,2}$ are expansion coefficients for the diabatic electronic states S_1 ($|1\rangle$) and S_2 ($|2\rangle$), respectively, and $(\mathbf{q}_t,\mathbf{p}_t)$ are the phase-space coordinates of the trajectory. The expansion coefficients evolve according to equations-of-motion derived from the TDSE,

$$\dot{\mathbf{a}} = -\frac{i}{\hbar}\left[\mathbf{H} - i\hbar\dot{\mathbf{S}}\right]\mathbf{a}\,. \tag{10}$$

Here, $\mathbf{H}$ is the Hamiltonian matrix in the electronic basis defined by $H_{ij} = \langle g_t|\,\langle i|\hat{H}|j\rangle\,|g_t\rangle$, and the elements of the time-derivative overlap matrix $\dot{\mathbf{S}}$ are

$$\dot{S}_{ij} = \delta_{ij}\left[\sum_{k=1}^{f}\left\langle g_t\,\middle|\,\frac{\partial g_t}{\partial q_k}\right\rangle\frac{\partial q_k}{\partial t} + \left\langle g_t\,\middle|\,\frac{\partial g_t}{\partial p_k}\right\rangle\frac{\partial p_k}{\partial t}\right]\ , \tag{11}$$

where the Dirac delta function arises due to the orthonormality of the electronic states. Initial positions and momenta of the sampling trajectories are obtained by sampling the Wigner phase-space distribution of the initial wavefunction, and these positions and momenta evolve

according to,

$$\frac{dq_k}{dt} = \frac{p_k}{m_k}\,, \tag{12}$$

$$\frac{dp_k}{dt} = -\frac{\partial V_{\rm Ehr}}{\partial q_k}\,, \tag{13}$$

where the Ehrenfest potential energy is given by

$$V_{\rm Ehr} = \frac{|a_1|^2 V_{11} + |a_2|^2 V_{22} + 2{\rm Re}(a_1^* a_2 V_{12})}{|a_1|^2 + |a_2|^2}\,, \tag{14}$$

with V_{ij} representing the element of the potential energy matrix of the system for electronic states i and j.

To account for the diabatic electronic states during basis sampling, GWPs are placed on electronic state $|1\rangle$ with a probability P_S^1, given by

$$P_S^1 = \frac{|a_1|^2}{|a_1|^2 + |a_2|^2}\,. \tag{15}$$

The probability of placing basis functions on state $|2\rangle$ is calculated in the same way, but using $|a_2|^2$ in the numerator. This approach to placing basis functions ensures that, near regions of configurational space in which the electronic states are strongly-coupled, GWPs are placed on both electronic surfaces.

The initial wavefunction for our calculations reflects photoexcitation of pyrazine from the ground state to the S_2 excited state, with the normal-mode vibrational coordinates all chosen as $q_\kappa = 0$. Specifically, the initial wavefunction is,

$$\psi(\mathbf{q}, t{=}0) = \left[\prod_{k=1}^{f} \left(\frac{1}{\pi}\right)^{1/4} \exp\left(-\frac{1}{2}q_k^2\right)\right] |2\rangle\ . \tag{16}$$

For the pyrazine model system considered here, the S_2 photoabsorption spectrum can be calculated by Fourier transform of the wavefunction autocorrelation function, enabling comparison with experimental data. However, our previous work has shown that, due to

the artificial dampening and sampling functions necessary to reproduce the resolution of the experimental spectrum, long-time dynamics are dampened to the point of having no effect on the final absorption spectrum at all;[44] in other words, the photoabsorption spectrum only assesses the accuracy of the simulation at short times in the pyrazine system. Instead, the state population dynamics provide a far more detailed insight into the accuracy with which the dynamics of the system are being reproduced;[44] as a result, we focus explicitly on calculating the diabatic population of S_1 as a measure of calculation accuracy. Within our propagation scheme, using the wavefunction of Eq. (4), the population $P_1(t)$ is given by,

$$P_1(t) = \sum_{i,j} c_i^*(t) c_j(t) \left\langle g_i(\mathbf{q}) \,|\, g_j(\mathbf{q}) \right\rangle \delta_{\lambda_i,1} \delta_{\lambda_j,1} \,, \tag{17}$$

where λ_j represents the state inhabited by basis function $|g_j(\mathbf{q})\rangle$.

Three calculations with differing initial basis set sizes were carried out, all employing a 0.1 fs timestep. The GWP basis sampling probability at each time-step was $1/n_s = 0.01$ during each calculation. Each trajectory sampling burst of 100 time-steps was immediately followed by 100 steps of wavefunction propagation; a set of 15 such trajectory-sampling bursts resulted in a total simulation time of 150 fs. MP optimization was carried out between each burst (*i.e.* every 10 fs) until the overlap of the optimized basis set with the wavefunction at the end of the previous burst reached $\Delta = 0.95$. The three calculations reported here employed different numbers of sampling trajectories, $m = 100, 300$ and 500, resulting in $\sim$1000, 3000 and 5000 GWP basis functions being sampled during each short sampling burst. The basis set sizes remained relatively constant throughout each simulation, with variations in number of GWPs retained by the MP algorithm being around 20%, 10% and 3% for initial sizes of 1000, 3000 and 5000 GWPs respectively; this is illustrated in Fig. 2, which shows the number of GWPs retained following MP optimization for the $m = 300$ simulation. All simulations used the fourth-order Runge-Kutta algorithm for propagation of the wavefunction expansion coefficients, while the velocity Verlet algorithm was used to

propagate the sampling trajectories. Finally, width parameters of all GWPs were fixed for all degrees of freedom at a value of $\gamma = 0.5$, reflecting the width of the initial wavepacket.

Fig. 3 shows the population of the S_1 state of pyrazine, $P_1(t)$, as a function of time for the three sizes of basis set employed. Even using just 1000 GWPs *per* short 10 fs propagation period, the qualitative features of the population dynamics are clearly reproduced by our method. The remaining error in Fig. 3(a) at longer times has two principal components. The first is due to the random nature of the initial conditions of the GWP sampling trajectories; in particular, we find that repeating the 1000 GWP simulations with different sets of GWP initial conditions leads to a variation of around 5% in the calculated population dynamics. The second aspect of the remaining error in Fig. 3(a) relates to the basis set size; as usual in basis set-based methods for wavefunction propagation, larger basis sets would be expected to give better agreement with the exact results because of the inherently better description of the wavefunction combined with the variational solution of the TDSE (at least for the expansion coefficients). Indeed, as expected, we find that increasing basis set size clearly allows for better description of some features of the population, such as the small re-absorbance to the S_2 state occurring after just a few femtoseconds; this is highlighted in Figs. 3(b) and 3(c). This suggest that our method quickly converges with respect to basis set size which, considering the small basis sets employed here, is very encouraging.

Further investigation of the oscillation at 10 fs highlights the role played by the duration of the trajectory bursts employed in our aTG method. To investigate further, Fig. 4 shows the populations arising from two calculations employing comparably sized basis sets ($N \simeq 3000$), but using different MP restart frequencies, namely 10 fs and 25 fs. The difference in behaviour between the calculations employing 10 fs bursts and 25 fs bursts, respectively, can be understood based on the effect of the burst duration on the basis set sampling during each period of propagation. First, consider the short time behaviour, where it is clear that using 25 fs burst trajectories gives more accurate results. The reason is due to the differing sizes of the basis set generated by classical sampling trajectories; in the case of 10 fs burst, GWP

sampling results in a total basis set size of 3064 which is used to propagate the wavefunction for the first 10 fs, although application of MP at 10 fs shows that only 7 of these GWPS make a significant contribution to the evolved wavefunction. In contrast, in the case of the 25 fs burst calculation, GWP sampling leads to a total GWP basis set size of 3252 GWPs which are used to propagate the wavefunction and, of these, we find that 297 GWPs are active after 25 fs. This comparison suggests that the effective active basis set generated by sampling GWPs with 25 fs bursts is larger and better spans the relevant region of phase-space than that generated by 10 fs bursts, leading to a more accurate calculation, as observed.

Now consider the behaviour at longer times, where 10 fs bursts are generally more accurate. Here, because of the shorter burst duration, the GWP sampling trajectories are, by definition, closer to the region of phase-space defined by the current evolving wavefunction; in contrast, the 25 fs burst trajectories will have more opportunity to explore a wider region of phase-space (due to the longer burst trajectory). Because these GWP trajectories are guided by classical-like equations-of-motion, there is no guarantee that the sampling generated by these longer 25 fs bursts will remain accurate with regards to evolution of the wavefunction, leading to larger errors in the calculation at longer simulation times. In contrast, we find that, after the initial time with errors arising as described above, the 10 fs burst trajectories lead to a more accurate result by sampling GWPs which are more relevant to the immediate time-evolution of the wavefunction. Finally, we note that, although one could argue that the same principle should apply at short times, a further difference between long- and short-time basis sets is the fact that, due to the application of the MP algorithm, the basis set at longer times can re-use some of the GWPs sampled at earlier times. For the initial sampling period (i.e. either 10 fs or 25 fs), this ability to re-use GWPs is obviously not possible and wavefunction evolution can only be based on those GWPs generated in the initial sampling period. As noted above, the 25 fs burst simulation enables a better exploration of phase-space in this initial period, leading to more accurate wavefunction propagation, although this advantage is lost at later times when the basis set generated by 25 fs bursts explores

regions of phase-space which are less directly relevant to propagation.

Fig. 5 compares the performance of the aTG algorithm presented here to the previous sTG version,[44] where long-time classical trajectories are used to sample GWP basis functions; shown are S_1 state populations for the 4-dimensional pyrazine Hamiltonian, compared to numerically-exact MCTDH results. Comparing the two results for approximately 3000 basis functions (bearing in mind that the MP optimisation algorithm results in an adaptive basis set of varying size) clearly illustrates the benefits of the modification presented here; while sTG results in relatively poor agreement in the population dynamics beyond 25 fs, the new aTG method yields qualitatively accurate dynamics across the entire time domain. Given that the main difference between the aTG and sTG methods is the use of short-time sampling trajectories, rather than serial long-time sampling, we believe that Fig. 5 highlights the problem of relying on classical trajectories at long times.

The benefits of our aTG modification can be even more clearly observed when comparing to data obtained using 2.4×10^4 basis functions within the original sTG formalism. Aside from the small divergence from the exact solution at around 10 fs, the origin of which has been noted above, using just 3000 GWPs during each 10 fs time period is sufficient to produce dynamics comparable in accuracy to that of the largest sTG calculation we have reported previously. Furthermore, if we compare the number of Hamiltonian matrix elements which must be evaluated in each different calculation as a way of comparing computational expense, we note that the aTG simulation with an average of 1000 GWP basis functions during each 10 fs time period requires just 3% of the Hamiltonian matrix element evaluations of the sTG method with a basis set size of 2.4×10^4 yet, as shown in Figs. 3 and 5, the population dynamics are of comparable accuracy.

The adaptive nature of the basis sets generated by our aTG method draws into question whether the basis set itself significantly increases in size during the simulation. Depending upon the nature of the underlying PES in a given problem, as well as the extent of phase-space which might be sampled for a given problem, one might expect that the number of basis

functions describing the wavefunction might fluctuate with time; in contrast, any *uncontrolled* growth of the number of basis functions would suggest that adaptive optimization by MP is not sufficient to maintain accurate description of the wavefunction. However, Fig. 6 shows that the MP scheme is capable of maintaining a steady overall basis set size, rather than a continuously growing basis; for a calculation with an initial basis set of 3000 GWPs, the total number of basis functions fluctuates at most by 10% about an average value of 3300 GWPs. Although not shown here, the calculations employing 1000 and 5000 basis functions behave similarly, with average variations of 20 % and 3% respectively.

Fig. 6 also shows the distribution of the basis set across the two diabatic electronic states, S_1 and S_2. As expected, the variation in the basis set occupancy on each state closely follows the calculated populations on the states. As a result, we find that our aTG scheme is capable of accurately modelling non-adiabatic dynamics on coupled electronic states; combining trajectory-guided sampling which spans both electronic states simultaneously with an adaptive scheme for basis optimization implicitly allows treatment of coupled electron-nuclear dynamics.

From the simulation results in this Section, we conclude that the relatively simple modifications to our previously published sTG method[44] reported here are highly effective in reducing the size of the active basis set required to converge to qualitative quantum dynamics. The MP optimisation algorithm used here can effectively maintain a minimal basis set which accurately represents the time-dependent wavefunction; the results in Fig. 5 and 6 demonstrate that the resulting dynamics of our aTG approach are accurate. Furthermore, we note that the underlying strategy of periodic basis set minimisation is highly transferable and should be readily applicable to other well established quantum simulation methods such as AIMS or MCE.

3.2 The double-well potential

Our aTG methodology is not just applicable to non-adiabatic systems; given that the new approach is less reliant on the accuracy of classical molecular dynamics at long times, it is interesting to investigate whether quantum tunnelling can also be correctly modelled using this procedure. Classical trajectories in themselves cannot accurately capture all quantum-mechanical tunnelling effects; however, by sampling from an initial quantum-mechanical distribution, classical trajectories have the potential to access regions of phase-space which are broadly consistent with quantum dynamics and so can be used to position basis functions appropriately. However, we stress that the final time-evolution of the system in our aTG method is performed according to variational solution of the TDSE.

To test our aTG method in the case of quantum tunnelling, we investigate a multidimensional double-well tunnelling benchmark which has been previously studied by several alternative quantum dynamics approaches.[57,61–63] This double-well model represents tunnelling of a quantum particle through a one-dimensional energy barrier; the tunnelling coordinate is itself coupled to a set of $f-1$ harmonic oscillators. The potential energy function is

$$V(\mathbf{q}) = V_{dw}(q_1) + V_{env}(\mathbf{q})\,, \tag{18}$$

where $V_{dw}(q_1)$ is the double-well potential given by

$$V_{dw}(q_1) = \frac{1}{16\eta}q_1^4 - \frac{1}{2}q_1^2\,, \tag{19}$$

and $V_{env}(\mathbf{q})$ is the remaining interaction representing the environment of harmonic oscillators and their coupling to the tunnelling coordinate q_1, as described below.

Here, we consider two different versions of this model, varying in the manner of coupling between tunnelling coordinate, q_1, and the bath modes. As in previous investigations of this

model,[57,61–63] we use $\eta = 1.3544$ and the initial wavefunction is a normalised GWP, given by

$$\psi_0(\mathbf{q}) = \prod_{k=1}^{f} \left(\frac{\alpha}{\pi\hbar}\right)^{1/4} \exp\left[-\frac{\alpha}{\hbar}(q_k - \bar{q}_k)^2\right] , \tag{20}$$

where f is the number of degrees of freedom, $\bar{q}_1 = -2.5$, $\bar{q}_j = 0$ for the other $f-1$ degrees-of-freedom, and $\alpha = 0.5$. In all simulations reported here, all degrees of freedom have mass $m = 1$.

The energy expectation value associated with this initial wavefunction is lower than the classical height of the barrier in the tunnelling coordinate for each of the three cases discussed below; as a result, tunnelling is an important factor in the dynamics of this system. To monitor the tunnelling dynamics, we calculate the tunnelling correlation function, $C_r(t)$, given by

$$C_r(t) = \langle \psi_r(\mathbf{q}, 0) \,|\, \psi(\mathbf{q}, t) \rangle , \tag{21}$$

where $\psi_r(\mathbf{q}, 0)$ is the mirror image of the initial wavefunction given in Eq. (20) (*i.e.* $\bar{q}_1 = +2.5$, $\bar{q}_j = 0$ for the other $f-1$ degrees-of-freedom). The magnitude of $C_r(t)$ describes the extent to which the wavefunction has tunnelled through the barrier.

3.2.1 Linear coupling

The first double-well potential considered here exhibits linear coupling between pairs of degrees-of-freedom, including the tunnelling coordinate q_1. The environmental contribution to the potential energy operator is

$$V_{env}(\mathbf{q}) = \sum_{i=2}^{f} \left[\frac{1}{2}q_i^2 + a q_{i-1} q_i\right] , \tag{22}$$

where $a = 0.2$.[62] We consider two version of this model, with $f = 2$ and $f = 5$; we refer to these hereafter as Model I and Model II. For both Model I and Model II, our calculations employed 12 bursts of trajectory sampling, each employing 10^4 time-steps of 0.002

a.u., resulting in 20 a.u. of total sampling time for each short-time period. In total, the wavefunction was propagated for 240 a.u.

Encouragingly, in the case of Model I, $m = 25$ sampling trajectories, storing basis functions with a probability of $1/n_s = 0.002$ at every time-step, were sufficient to obtain numerical accuracy with respect to configuration interaction (CI) benchmark results,[62] as shown in Fig. 7(a). The resulting adaptive basis set, which was optimised with a MP convergence of $\Delta = 0.99$, had an average size of 517 GWPs with variation between bursts not exceeding 10% of this value. The consistency of the basis set size again shows that our method is not simply reliant on stepwise expansion of the basis set to maintain accuracy.

In the case of Model II, the additional bath modes require a larger basis set to achieve accurate results, as expected. Here, we employed $m = 50$ sampling trajectories with storage probability $1/n_s = 0.008$, resulting in an average basis set size of 1032 GWPs. MP optimization employed a cut-off of $\Delta = 0.995$, which resulted in an encouragingly consistent basis set size, with variations remaining below 14%. As shown in Fig. 7(b), our method is able to qualitatively reproduce the tunnelling dynamics, with the main inconsistency appearing in the higher frequency oscillations of the tunnelling correlation function, $C_r(t)$. Increasing the basis set size further improves the reproduction of the exact results, as expected; for example, a simulation employing 5000 GWPs on average is shown in Fig. 7(c),(although there remains some error due to this finite basis set). Overall these results are highly encouraging as they provide further evidence that the aTG method outlined here can be used to treat quantum dynamics in tunnelling systems, despite being founded on purely classical trajectories.

3.2.2 Quadratic coupling

In the final case, termed Model III, coupling to the bath modes is quadratic in nature; additionally, coupling occurs between the tunnelling coordinate q_1 and all modes constituting the harmonic bath, not just between q_1 and q_2 as in Eq. 22. The nature of this coupling

means that the effective potential experienced along the q_1 tunnelling coordinate is strongly asymmetric, with one potential energy well being lower in energy than the other; we find that this feature means that the quantum dynamics of Model III are significantly more difficult to reproduce in trajectory-based schemes than either Models I or II.

The coupling and bath potential for Model III is given by

$$V_{env}(\mathbf{q}) = \sum_{i=2}^{f} \left[\frac{1}{2} q_i^2 + a q_1 q_i^2 \right] , \tag{23}$$

where $a = 0.05$ and $f = 20$.[62] Again, the mass is $m = 1$ for all degrees-of-freedom. In our aTG simulations we used a set of $m = 50$ sampling trajectories, with a 0.002 a.u. timestep and a sampling probability of $1/n_s = 0.005$. Our simulation comprised 60 bursts of trajectory sampling, each lasting 1000 timesteps, resulting in a total propagation time of 120 a.u.. MP optimisation was carried out using a cut-off value of $\Delta = 0.995$, yielding a basis set comprising an average of 884 GWPs. The basis set size varied by a maximum of 44%, although the average variation across the full simulation time was just 5%. For comparison, we also performed a sTG simulation using comparable simulation conditions. In particular, we initiated 50 independent trajectories of 60×10^3 timesteps, placing basis functions with a probability of $1/n_s = 0.00025$; this results in a total basis set size of 994 GWPs (*i.e.* directly comparable to our aTG simulation), and the expansion coefficients of this set were propagated using Eq. 5 with a tilmestep of 0.002 a.u..

We note that, following other GWP simulations of this model,[63] we sample initial GWP positions at $t = 0$ from both the initial wavefunction and its mirror image $\psi_r(\mathbf{q}, 0)$ in both aTG and sTG simulations; this approach to sampling GWPs is only used in our approach at $t = 0$, while initial GWP conditions are sampled form the time-evolving wavefunction during later short-time trajectory sampling periods. Without this sampling approach, classical trajectory-based methods do not exhibit sufficient tunnelling through the double-well barrier as a result of the strongly asymmetric nature of the potential; this is discussed further below.

The results shown in Fig. 8 clearly reflect the differences between our original sTG approach and the updated aTG method. Specifically, sTG fails to qualitatively reproduce the tunnelling dynamics; in particular, sTG overestimates the extent of tunnelling through the double-well potential, a feature which is most likely an artefact of the initial generation of GWP sampling trajectories which, as noted above, are sampled from both sides of the double-well potential along q_1. In contrast, aTG does a reasonable job of reproducing the magnitude of tunnelling through the double-well barrier. The aTG dynamics is correctly reproduced for times up to around $t = 25$ a.u. (Fig. 8 (a)); however, we note that this is sufficient to capture the initial tunnelling dynamics, despite our approach being based solely on classical trajectories. At longer times, our calculated $C_r(t)$ broadly follows the exact result, although with a noticeable decrease in the magnitude of oscillations in the correlation function; this suggests that, at medium-to-long times, the wavefunction approximated by our approach is does not tunnel sufficiently. The spectrum (Fig. 8(b)), obtained *via* Fourier transform of $C_r(t)$ in the same procedure outlined in our previous work,[44] reflects the results of Fig. 8(a); the dynamics are qualitatively correct, but some of the details are inaccurate.

These results serve to first emphasize the significant advantage of adopting an adaptive basis strategy. Here, any given time-propagation period has around 900 GWPs in both the aTG and sTG simulations, but the aTG results are much more qualitatively accurate due to the adaptation of the trajectories to the current wavefunction; in other words, by periodically optimizing the basis and reinitialising trajectories based on the phase-space of the current wavefunction, the short-time sampling of GWPs is much more representative of the space to be spanned by the wavefunction in the near-future. However, although basis re-sampling and adaptation is clearly advantageous, the reliance on classical trajectories remains; this fact explains the remaining errors in our aTG simulations. Because these classical sampling trajectories do not capture quantum effects such as tunnelling, a clear route to improving our methodology would be to move towards sampling methods which do include such effects; examples here might include ring-polymer molecular dynamics (RPMD[64,65]) or

centroid molecular dynamics (CMD[66,67]), and work in this direction is now under way.

4 Conclusions

In this Article, we have addressed the limitations of our previously-published sTG trajectory sampling method for quantum dynamics simulations.[44] Specifically we have proposed a simple modification which alleviated problems associated with divergence of the sampling trajectories at long times, which previously resulted in in inefficient basis set sizes and poor computational scaling. Here, in our aTG approach, by limiting the duration of the sampling steps, as well as minimising and optimising the active basis set during propagation, these challenges can be alleviated.

To demonstrate the effectiveness of adaptive trajectory approach, we have studied challenging multidimensional quantum dynamics benchmark problems. The vibronic pyrazine Hamiltonian allowed for direct comparison to the serial trajectory sampling method and showed that comparable accuracy can be achieved with basis sets only a fraction of size required in our original trajectory-based approach. To further show the applicability of this approach to larger systems, we also explored a double-well tunnelling benchmark problem.[57,61–63] Again in the case of few degrees of freedom, our method was shown to be accurate and efficient. In the higher dimensional case, whilst observing some loss of accuracy, we were still able to capture qualitative dynamics at reasonable computational cost. These results are extremely encouraging given the simplicity of our approach and its grounding in classical mechanics. As noted above, strongly quantum mechanical problems, such as tunnelling through strongly asymmetric barriers (Model III) are still a challenge, although we note that aTG is very successful in capturing the qualitative dynamics of the system; current work is focussed on replacing the classical trajectory sampling with path integral-based approaches which are computationally efficient yet captures the role of quantum-mechanical tunnelling on the sampled configurations of the GWP basis functions, and we expect that such an

approach will help to further improve our overall adaptive quantum simulation strategy.

Acknowledgements

The authors gratefully acknowledge the EPSRC for award of funding to MACS. Computing facilities were provided by the Scientific Computing Research Technology Platform of the University of Warwick. Data for Figures 2-8 can be accessed at http://wrap.warwick.ac.uk/id/eprint/84832.

References

(1) Schrödinger, E. An Undulatory Theory of the Mechanics of Atoms and Molecules. *Phys. Rev.* **1926**, *28*, 1049–1070.

(2) Park, T. J.; Light, J. C. Unitary quantum time evolution by iterative Lanczos reduction. *J. Chem. Phys.* **1986**, *85*, 5870–5876.

(3) Schmidt, P. P. Harmonic oscillator basis functions and Gaussian model potentials for the analysis of anharmonic vibrations*. *Int. J. Quantum Chem.* **2002**, *90*, 202–226.

(4) Sielk, J.; von Horsten, H. F.; Kruger, F.; Schneider, R.; Hartke, B. Quantum-mechanical wavepacket propagation in a sparse, adaptive basis of interpolating Gaussians with collocation. *Phys. Chem. Chem. Phys.* **2009**, *11*, 463–475.

(5) Dirac, P. A. M. Note on Exchange Phenomena in the Thomas Atom. *Math. Proc. Cam. Phil. Soc.* **1930**, *26*, 376–385.

(6) Frenkel, J. *Wave Mechanics*; Oxford University Press: Oxford, 1934.

(7) McLachlan, A. A variational solution of the time-dependent Schrodinger equation. *Mol. Phys.* **1964**, *8*, 39–44.

(8) Broeckhove, J.; Lathouwers, L.; Kesteloot, E.; Leuven, P. V. On the equivalence of time-dependent variational principles. *Chem. Phys. Lett.* **1988**, *149*, 547 – 550.

(9) Gu, B.; Garashchuk, S. Quantum Dynamics with Gaussian Bases Defined by the Quantum Trajectories. *J. Phys. Chem. A* **2016**, *120*, 3023–3031, PMID: 26735750.

(10) Meyer, H.-D.; Gatti, F.; Worth, G. *Multidimensional quantum dynbamics: MCTDH theory and applications*; Wiley: Winheim, Germany, 2009.

(11) Meyer, H.-D.; Manthe, U.; Cederbaum, L. The multi-configurational time-dependent Hartree approach. *Chem. Phys. Lett.* **1990**, *165*, 73 – 78.

(12) Burghardt, I.; Meyer, H.-D.; Cederbaum, L. S. Approaches to the approximate treatment of complex molecular systems by the multiconfiguration time-dependent Hartree method. *J. Chem. Phys.* **1999**, *111*, 2927–2939.

(13) Raab, A.; Worth, G. A.; Meyer, H.-D.; Cederbaum, L. S. Molecular dynamics of pyrazine after excitation to the S2 electronic state using a realistic 24-mode model Hamiltonian. *J. Chem. Phys.* **1999**, *110*, 936–946.

(14) Burghardt, I.; Giri, K.; Worth, G. A. Multimode quantum dynamics using Gaussian wavepackets: The Gaussian-based multiconfiguration time-dependent Hartree (G-MCTDH) method applied to the absorption spectrum of pyrazine. *J. Chem. Phys.* **2008**, *129*, 174104.1–174104.14.

(15) Burghardt, I.; Nest, M.; Worth, G. A. Multiconfigurational system-bath dynamics using Gaussian wave packets: Energy relaxation and decoherence induced by a finite-dimensional bath. *J. Chem. Phys.* **2003**, *119*, 5364–5378.

(16) Worth, G. A.; Burghardt, I. Full quantum mechanical molecular dynamics using Gaussian wavepackets. *Chem. Phys. Lett.* **2003**, *368*, 502 – 508.

(17) Worth, G. A.; Robb, M. A.; Burghardt, I. A novel algorithm for non-adiabatic direct dynamics using variational Gaussian wavepackets. *Faraday Discuss.* **2004**, *127*, 307–323.

(18) Römer, S.; Burghardt, I. Towards a variational formulation of mixed quantum-classical molecular dynamics. *Mol. Phys.* **2013**, *111*, 3618–3624.

(19) Römer, S.; Ruckenbauer, M.; Burghardt, I. Gaussian-based multiconfiguration time-dependent Hartree: A two-layer approach. I. Theory. *J. Chem. Phys.* **2013**, *138*.

(20) Preston, R. K.; Tully, J. C. Effects of Surface Crossing in Chemical Reactions: The H3+ System. *J. Chem. Phys.* **1971**, *54*, 4297–4304.

(21) Tully, J. C.; Preston, R. K. Trajectory Surface Hopping Approach to Nonadiabatic Molecular Collisions: The Reaction of H+ with D2. *J. Chem. Phys.* **1971**, *55*, 562–572.

(22) Tully, J. C. Molecular dynamics with electronic transitions. *J. Chem. Phys.* **1990**, *93*, 1061–1071.

(23) Martinez, T. J.; Ben-Nun, M.; Levine, R. D. Multi-Electronic-State Molecular Dynamics:â A Wave Function Approach with Applications. *J. Phys. Chem.* **1996**, *100*, 7884–7895.

(24) Ben-Nun, M.; MartÄ±Ìnez, T. J. Nonadiabatic molecular dynamics: Validation of the multiple spawning method for a multidimensional problem. *J. Chem. Phys.* **1998**, *108*, 7244–7257.

(25) Ben-Nun, M.; Martinez, T. J. Ab Initio Quantum Molecular Dynamics. *Adv. Chem. Phys.* **2002**, *121*, 439.

(26) Ben-Nun, M.; MartÄ±Ìnez, T. J. Nonadiabatic molecular dynamics: Validation of the multiple spawning method for a multidimensional problem. *J. Chem. Phys.* **1998**, *108*, 7244–7257.

(27) Ben-Nun, M.; Quenneville, J.; Martínez, T. J. Ab Initio Multiple Spawning:â Photochemistry from First Principles Quantum Molecular Dynamics. *J. Phys. Chem. A* **2000**, *104*, 5161–5175.

(28) Shalashilin, D. V. Quantum mechanics with the basis set guided by Ehrenfest trajectories: Theory and application to spin-boson model. *J. Chem. Phys.* **2009**, *130*, 244101.

(29) Shalashilin, D. V. Nonadiabatic dynamics with the help of multiconfigurational Ehrenfest method: Improved theory and fully quantum 24D simulation of pyrazine. *J. Chem. Phys.* **2010**, *132*, 244111.

(30) Makhov, D. V.; Glover, W. J.; Martinez, T. J.; Shalashilin, D. V. Ab initio multiple cloning algorithm for quantum nonadiabatic molecular dynamics. *J. Chem. Phys.* **2014**, *141*, 054110.

(31) Li, X.; Iyengar, S. S. Quantum Wavepacket Ab Initio Molecular Dynamics for Extended Systems. *J. Phys. Chem. A* **2011**, *115*, 6269–6284.

(32) Li, X.; Iyengar, S. S. Quantum wavepacket ab initio molecular dynamics: Generalizations using an extended Lagrangian treatment of diabatic states coupled through multireference electronic structure. *J. Chem. Phys.* **2010**, *133*, 184105.

(33) Li, J.; Li, X.; Iyengar, S. S. Vibrational Properties of Hydrogen-Bonded Systems Using the Multireference Generalization to the "On-the-Fly" Electronic Structure within Quantum Wavepacket ab Initio Molecular Dynamics (QWAIMD). *J. Chem. Theory Comput.* **2014**, *10*, 2265–2280.

(34) Wang, H.; Sun, X.; Miller, W. H. Semiclassical approximations for the calculation of thermal rate constants for chemical reactions in complex molecular systems. *J. Chem. Phys.* **1998**, *108*, 9726–9736.

(35) Sun, X.; Wang, H.; Miller, W. H. Semiclassical theory of electronically nonadiabatic dynamics: Results of a linearized approximation to the initial value representation. *J. Chem. Phys.* **1998**, *109*, 7064–7074.

(36) Miller, W. H. The Semiclassical Initial Value Representation: A Potentially Practical Way for Adding Quantum Effects to Classical Molecular Dynamics Simulations. *J. Phys. Chem. A* **2001**, *105*, 2942–2955.

(37) Miller, W. H. On the Relation between the Semiclassical Initial Value Representation and an Exact Quantum Expansion in Time-Dependent Coherent States. *J. Phys. Chem. B* **2002**, *106*, 8132.

(38) Liu, J.; Miller, W. H. Linearized semiclassical initial value time correlation functions using the thermal Gaussian approximation: Applications to condensed phase systems. *J. Chem. Phys.* **2007**, *127*, 114506.

(39) Miller, W. H. Electronically Nonadiabatic Dynamics via Semiclassical Initial Value Methods. *J. Phys. Chem. A* **2009**, *113*, 1405–1415.

(40) Sun, X.; Miller, W. H. Forward–backward initial value representation for semiclassical time correlation functions. *J. Chem. Phys.* **1999**, *110*, 6635–6644.

(41) Thoss, M.; Wang, H.; Miller, W. H. Generalized forward–backward initial value representation for the calculation of correlation functions in complex systems. *J. Chem. Phys.* **2001**, *114*, 9220–9235.

(42) Liu, J.; Miller, W. H.; Paesani, F.; Zhang, W.; Case, D. A. Quantum dynamical effects in liquid water: A semiclassical study on the diffusion and the infrared absorption spectrum. *J. Chem. Phys.* **2009**, *131*, 164509.

(43) Habershon, S. Linear dependence and energy conservation in Gaussian wavepacket basis sets. *J. Chem. Phys.* **2012**, *136*, 014109.1–014109.8.

(44) Saller, M. A. C.; Habershon, S. Basis set generation for quantum dynamics simulations using simple trajectory-based methods. *J. Chem. Theory Comput.* **2015**, *11*, 8–16.

(45) Koch, W.; Frankcombe, T. J. Basis Expansion Leaping: A New Method to Solve the Time-Dependent Schrödinger Equation for Molecular Quantum Dynamics. *Phys. Rev. Lett.* **2013**, *110*, 263202.

(46) Wu, Y.; Batista, V. S. Matching-pursuit for simulations of quantum processes. *J. Chem. Phys.* **2003**, *118*, 6720–6724.

(47) Chen, X.; Batista, V. S. Matching-pursuit/split-operator-Fourier-transform simulations

of excited-state nonadiabatic quantum dynamics in pyrazine. *J. Chem. Phys.* **2006**, *125*, 124313.

(48) Prociuk, A. H.; Iyengar, S. S. A Multiwavelet Treatment of the Quantum Subsystem in Quantum Wavepacket Ab Initio Molecular Dynamics through an Hierarchical Partitioning of Momentum Space. *J. Chem. Theory Comput.* **2014**, *10*, 2950–2963.

(49) Polyak, I.; Allan, C. S. M.; Worth, G. A. A complete description of tunnelling using direct quantum dynamics simulation: Salicylaldimine proton transfer. *J. Chem. Phys.* **2015**, *143*, 084121.

(50) Müller, U.; Stock, G. Flow of zero-point energy and exploration of phase space in classical simulations of quantum relaxation dynamics. II. Application to nonadiabatic processes. *J. Chem. Phys.* **1999**, *111*, 77–88.

(51) Golosov, A. A.; Reichman, D. R. Classical mapping approaches for nonadiabatic dynamics: Short time analysis. *J. Chem. Phys.* **2001**, *114*, 1065–1074.

(52) Berkelbach, T. C.; Reichman, D. R.; Markland, T. E. Reduced density matrix hybrid approach: An efficient and accurate method for adiabatic and non-adiabatic quantum dynamics. *J. Chem. Phys.* **2012**, *136*, 034113.

(53) Mallat, S.; Zhang, Z. Matching pursuits with time-frequency dictionaries. **1993**, *41*, 3397–3415.

(54) Martinez, T. J.; Levine, R. D. Non-adiabatic molecular dynamics: Split-operator multiple spawning with applications to photodissociation. *J. Chem. Soc. Farad. Trans.* **1997**, *93*, 941–947.

(55) Martínez, T. J.; Ben-Nun, M.; Levine, R. D. Molecular Collision Dynamics on Several Electronic States. *J. Phys. Chem. A* **1997**, *101*, 6389–6402.

(56) Habershon, S.; Manolopoulos, D. E. Zero point energy leakage in condensed phase dynamics: An assessment of quantum simulation methods for liquid water. *J. Chem. Phys.* **2009**, *131*, 244518.

(57) Wu, Y.; Batista, V. S. Quantum tunneling dynamics in multidimensional systems: A matching-pursuit description. *J. Chem. Phys.* **2004**, *121*, 1676–1680.

(58) Yamazaki, I.; Murao, T.; Yamanaka, T.; Yoshihara, K. Intramolecular electronic relaxation and photoisomerization processes in the isolated azabenzene molecules pyridine, pyrazine and pyrimidine. *Faraday Discuss. Chem. Soc.* **1983**, *75*, 395–405.

(59) Innes, K.; Ross, I.; Moomaw, W. R. Electronic states of azabenzenes and azanaphthalenes: A revised and extended critical review. *J. Mol. Spectrosc.* **1988**, *132*, 492 – 544.

(60) Sala, M.; Saab, M.; Lasorne, B.; Gatti, F.; Guérin, S. Laser control of the radiationless decay in pyrazine using the dynamic Stark effect. *J. Chem. Phys.* **2014**, *140*, 194309.

(61) Sherratt, P. A.; Shalashillin, D. V.; Child, M. S. Description of multidimensional tunnelling with the help of coupled coherent states guided by classical Hamiltonians with quantum corrections. *Chem. Phys.* **2006**, *322*, 127 – 134.

(62) Habershon, S. Trajectory-guided configuration interaction simulations of multidimensional quantum dynamics. *J. Chem. Phys.* **2012**, *136*, 054109.

(63) Green, J. A.; Grigolo, A.; Ronto, M.; Shalashilin, D. V. A two-layer approach to the coupled coherent states method. *J. Chem. Phys.* **2016**, *144*.

(64) Craig, I. R.; Manolopoulos, D. E. Quantum statistics and classical mechanics: Real time correlation functions from ring polymer molecular dynamics. *J. Chem. Phys.* **2004**, *121*, 3368–3373.

(65) Habershon, S.; Manolopoulos, D. E.; Markland, T. E.; Miller, T. F. Ring-Polymer Molecular Dynamics: Quantum Effects in Chemical Dynamics from Classical Trajectories in an Extended Phase Space. *Annu. Rev. Phys. Chem.* **2013**, *64*, 387–413, PMID: 23298242.

(66) Geva, E.; Shi, Q.; Voth, G. A. Quantum-mechanical reaction rate constants from centroid molecular dynamics simulations. *J. Chem. Phys.* **2001**, *115*, 9209–9222.

(67) Voth, G. A. Path-Integral Centroid Methods in Quantum Statistical Mechanics and Dynamics. *Adv. Chem. Phys.* **2007**, *93*, 135–218.

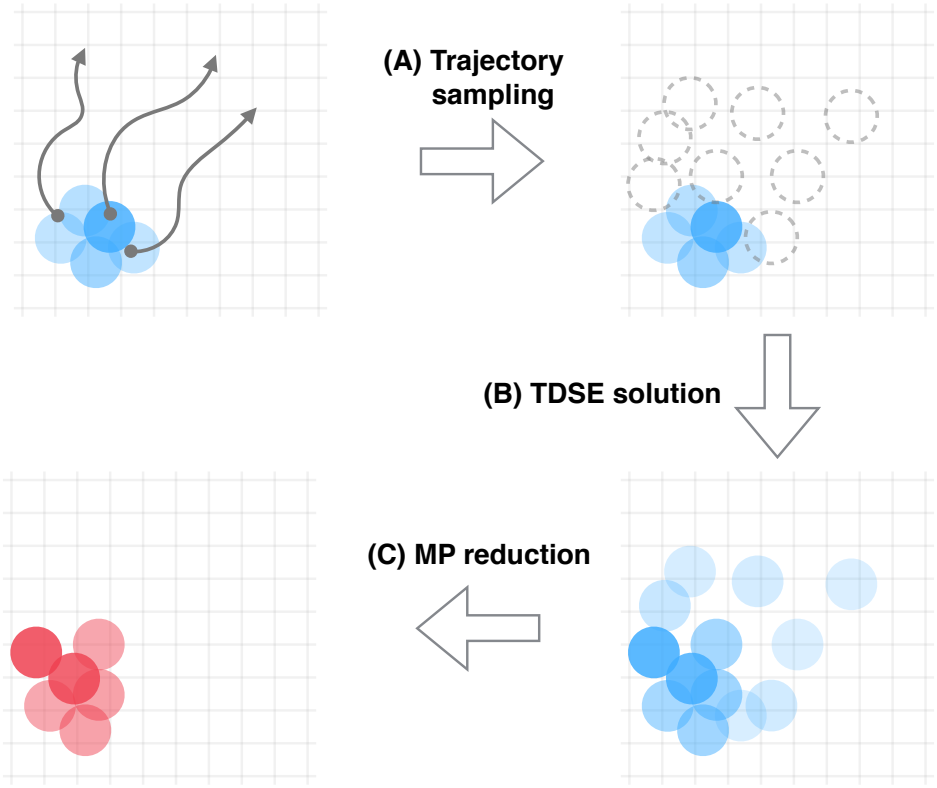

Figure 1: Schematic outline of aTG algorithm. Starting from an initial wavefunction expanded in a set of GWPs, new GWPs are added to the basis set by trajectory sampling (A). Solution of the TDSE for the full set of GWPs (B), followed by reduction by the MP method (C) results in a time-propagated wavefunction described by a minimal set of GWPs.

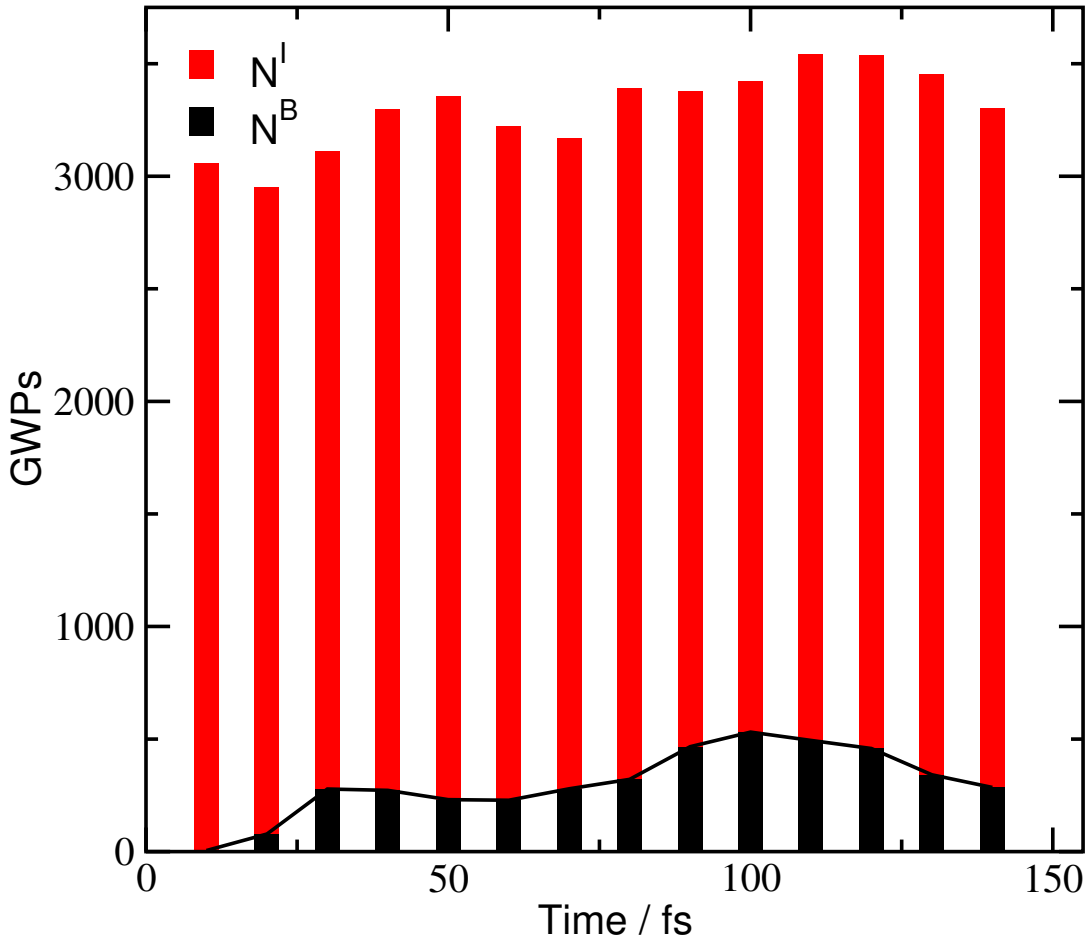

Figure 2: Comparison of initial basis set size, N^I, to the size of the set resulting from the MP optimisation and minimisation algorithm ($\Delta = 0.95$), N^B, for the 4-dimensional vibronic pyrazine Hamiltonian.

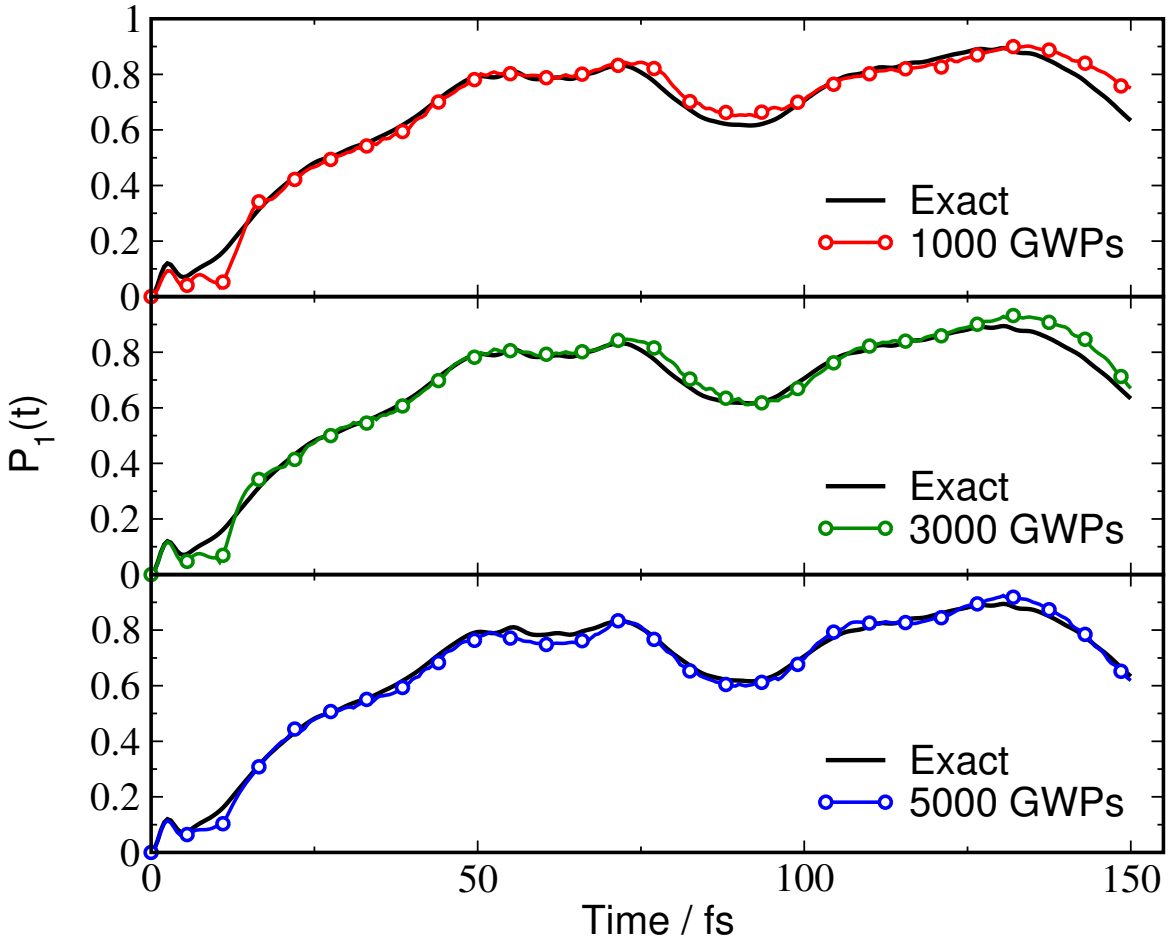

Figure 3: Population of the lower diabatic S_1 state, $P_1(t)$, as a function of time, calculated using adaptive basis sets with varying size, for the 4D pyrazine Hamiltonian. The basis set sizes given are approximately the number of GWPs which form the wavefunction during each short 10 fs propagation period.

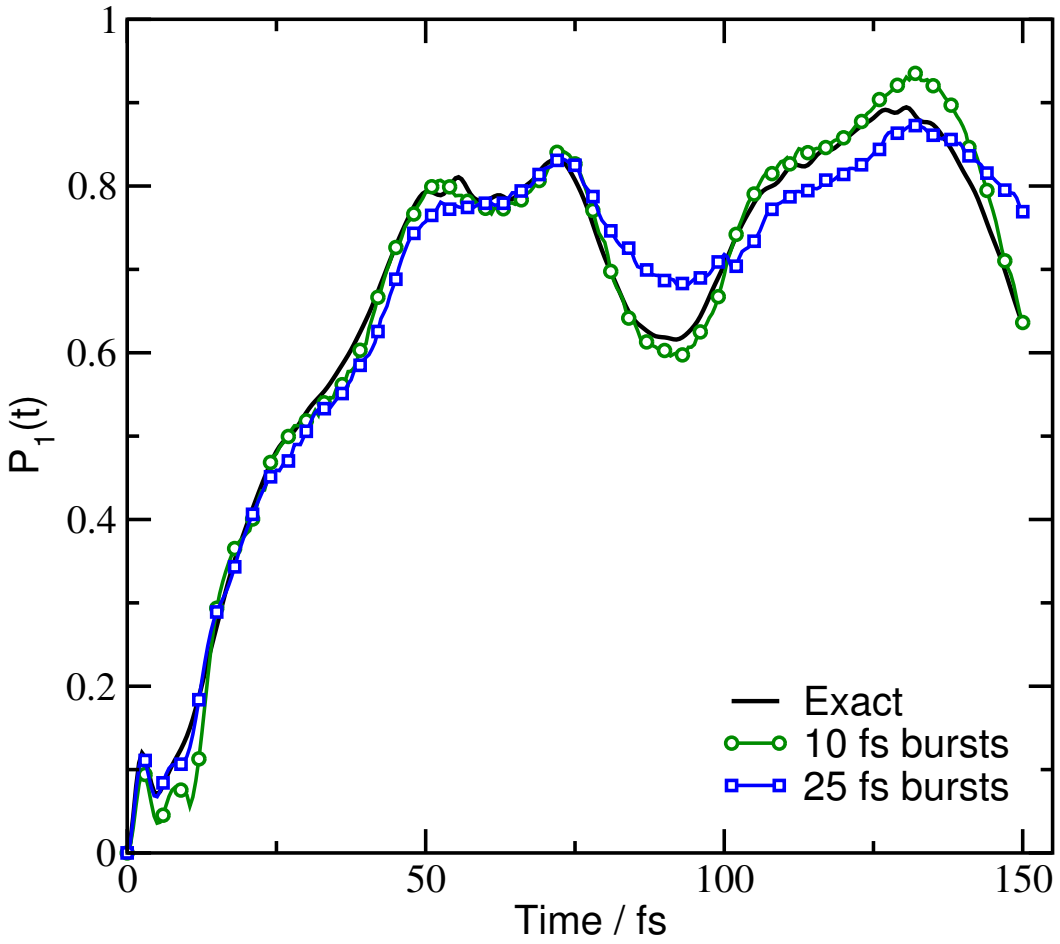

Figure 4: Population of the lower diabatic S_1 state, $P_1(t)$, as a function of time, for the 4D pyrazine Hamiltonian using different MP restart frequencies.

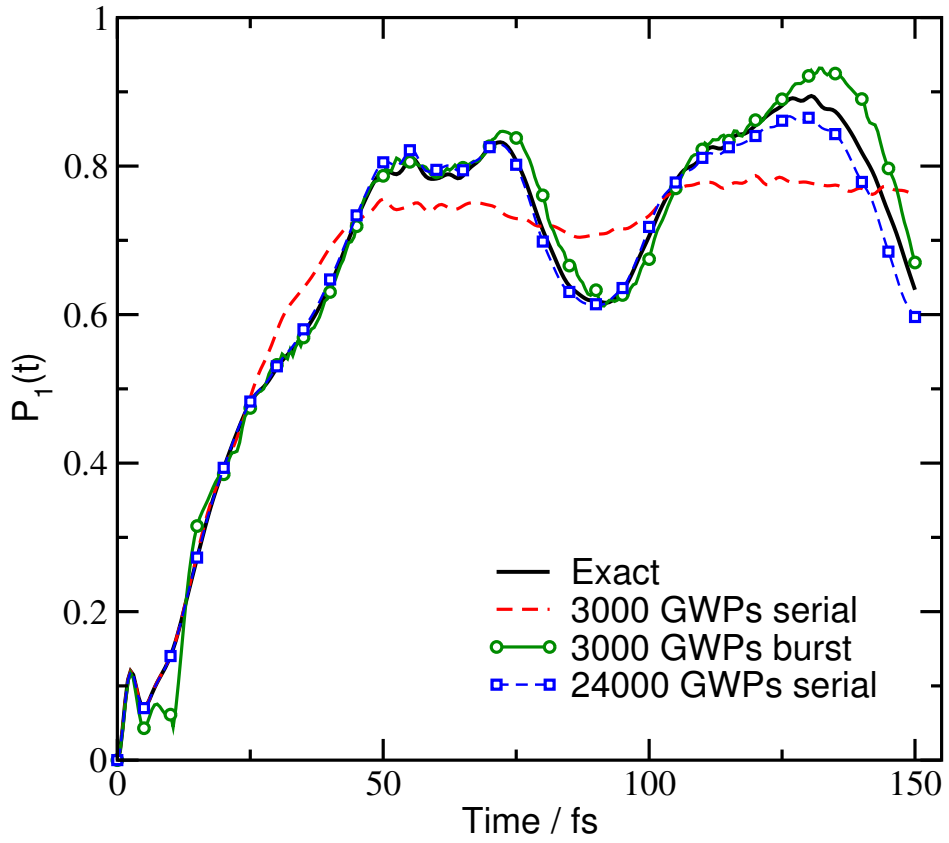

Figure 5: Population of the S_1 state, calculated using the trajectory burst sampling algorithm presented herein as well as the previously published[44] serial approach.

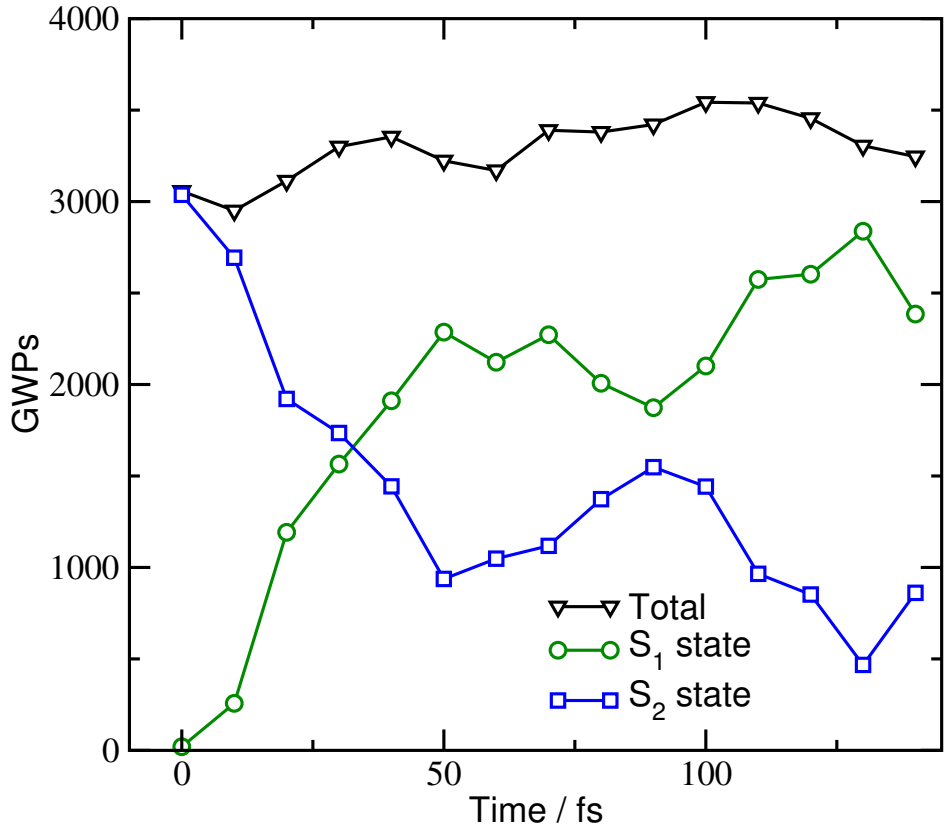

Figure 6: Size of the adaptive basis set for a calculation starting with 3000 GWPs, as well as explicit GWP state populations.

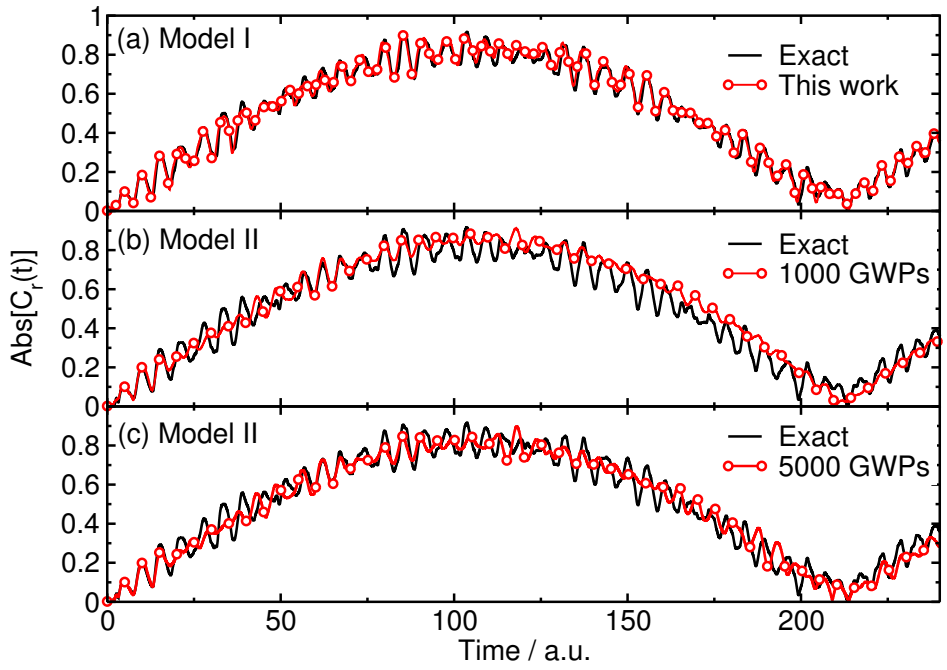

Figure 7: Tunnelling correlation functions for (a) Model I ($f = 2$), (b) Model II ($f = 5$) using 1000 GWPs and (c) Model III using 5000 GWPs compared to CI benchmark.[62]

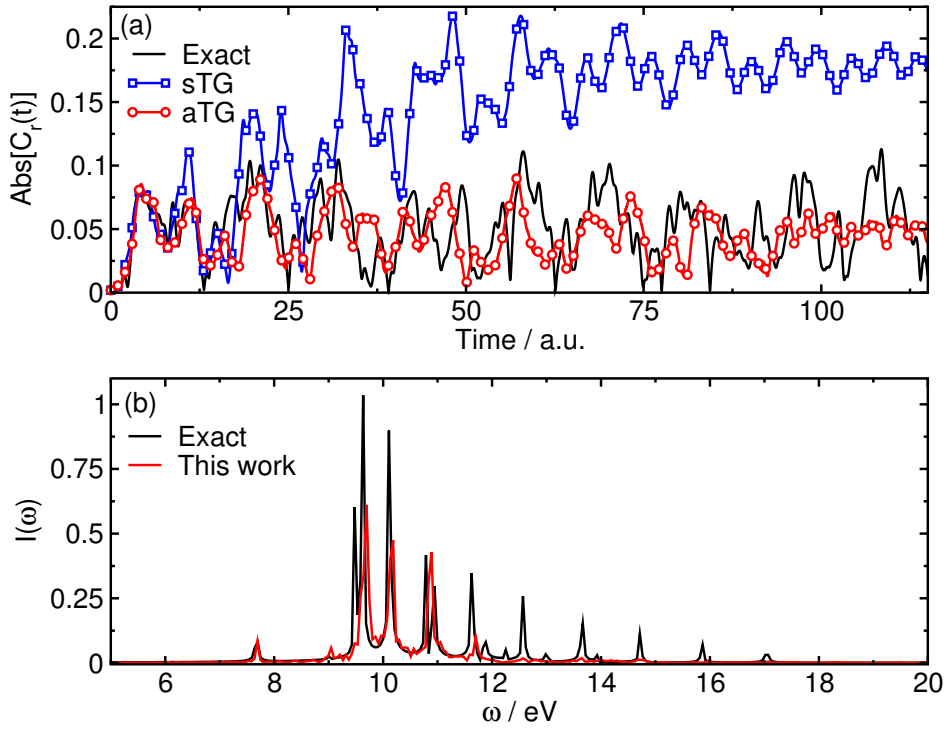

Figure 8: (a) Tunnelling correlation function for Model III ($f = 20$), (b) corresponding spectrum obtained via Fourier transform

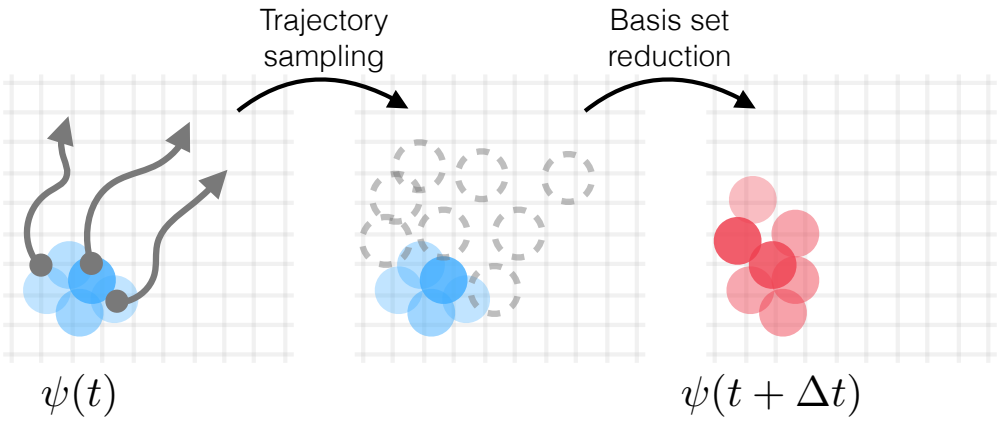

Figure 9: Table of Contents graphic